Journal of the Meteorological Society of Japan

EARLY ONLINE RELEASE

This is a PDF of a manuscript that has been peer-reviewed and accepted for publication. As the article has not yet been formatted, copy edited or proofread, the final published version may be different from the early online release.

The DOI for this manuscript is
DOI:10.2151/jmsj.2022-032
J-STAGE Advance published date: April 14th, 2022
The final manuscript after publication will replace the preliminary version at the above DOI once it is available.

Robust and Uncertain Sea-Level Pressure Patterns over Summertime East Asia in the CMIP6 Multi-Model Future Projections

Tomoaki OSE[1], Hirokazu ENDO[1], Yuhei TAKAYA[1], Shuhei MAEDA[2]
and
Toshiyuki NAKAEGAWA[1]

1) Meteorological Research Institute, Tsukuba, Japan

2) Japan Meteorological Agency, Tokyo, Japan

December 26, 2021: Submitted to JMSJ
February 15, 2022: Revised
March 30, 2022: Final

Corresponding author: Tomoaki Ose, Meteorological Research Institute,
1-1 Nagamine, Tsukuba, Ibaraki, 305-0052 JAPAN
Email: tomoaose@mri-jma.go.jp
Tel: +81-29-853-8647

Abstract

Robust and uncertain sea-level pressure patterns over summertime East Asia in the future global warming projections and their causes are studied by applying the inter-model empirical orthogonal function (EOF) analysis to the multi-model experiments in the sixth phase of the Coupled Model Intercomparison Project (CMIP6) and focusing common features with the previous CMIP5 analysis. The ensemble average and the first to third EOF modes associated with future pressure changes are similar to the corresponding ones from CMIP5. The first and second modes represent strengthened and weakened high pressure systems in subtropical and northern East Asia, respectively. The third mode is the reverse anomaly of the climatological pressure pattern over summertime East Asia, indicating weakened southerly monsoon winds. The second mode pattern makes positive contributions to almost all the CMIP6 future pressure changes, representing a robust future projection pattern. The robust mode is the result of surface warming over the northern continents and neighboring seas that is stronger than the global average. The first and third modes are considered to be uncertain (but major) patterns in the ensemble projections because the signs of their contributions to the future changes are dependent on the model used. Suppressed vertical motion over the equatorial (northern) Indian Ocean caused by the vertically stabilized atmosphere under the global warming scenario is the source of the first (third) mode, together with the counter vertical motion anomaly over the equatorial (northern) Pacific. The above characteristics of the modes are essentially similar to those identified in the CMIP5 analysis while different sea surface temperature anomalies are related to the secondary structures of the modes. Some uncertainties in the future projections can be attributed to the systematic differences in the model climatology of the present-day precipitation, which determines the distribution of the suppressed vertical motion under the future warmer climate.

Keywords: global warming; summertime East Asia; CMIP6; sea-level pressure; Asian monsoon

1. Introduction

Future changes to the East Asian summer climate such as surface air temperature and rainfall are causing concern with respect to their impacts on agriculture, health, and other social and economic factors. Therefore, this issue has been the focus of numerous studies (e.g., Kitoh et al. 1997; Kimoto 2005; Ueda et al. 2006), the results of which are basically consistent with the "wet-getting-wetter" effect (Held and Soden 2006). In contrast, Zou et al. (2017) concluded that the uncertainty associated with the fifth phase of the Coupled Model Intercomparison Project (CMIP5) future projections (Taylor et al. 2012) with respect to East Asian summer precipitation was caused by the uncertainty associated with atmospheric circulation changes. This is also the case for future projections generated using the 60-km-resolution Meteorological Research Institute-Atmospheric General Circulation Model (MRI-AGCM60; Mizuta et al. 2012) with different cumulus schemes under the prescribed future sea surface temperature (SST; Ose 2017). Explaining the differences and similarities among the multi-model projections in a physical sense is key to obtaining appropriately confident future projections and further improving climate modeling.

The significantly different effects of land and ocean on future changes in the summertime Asian monsoon have been clearly shown (e.g., Kamae et al. 2014; Endo et al. 2018; He and Zhou 2020). Endo et al. (2018) analyzed two types of the CMIP5 multi-model experiments: one was a global warming experiment, but with SST fixed to the present day, whereas the other was a present-day experiment, but under a future global warming SST. In the former experiment to determine the effects of warming land, the northward expansion of the Asian monsoon circulation was simulated with southerly winds strengthening over the East Asian continent and neighboring seas. For the latter experiment for the effects of warmer SST, the weakened monsoon circulation was simulated with suppressed vertical motion over the Indian and Pacific oceans.

The changes in many processes within climate systems are involved in the results of climate model experiment. To understand the similarities and differences among the many future climate projections, the likely changes in these elementary processes, which form the basis of the models, must also be understood. Ose et al. (2020) used empirical orthogonal function (EOF) analysis to investigate future changes in summertime East Asian sea-level pressure patterns from the 38 CMIP5 projections for the RCP8.5 scenario with the aim of identifying a storyline approach to the future regional circulation and climate (Shepherd 2019). The EOF study gives the possibility to know which of forcings and elements quantitatively dominate the inter-model differences among a large ensemble of future projections over the EOF region. This point is critically different from the previously referred studies. Ose et al. (2020) focused on the future changes in surface air temperature and vertical motion as the sources of the EOF modes because the land–sea contrast in surface air temperature is a fundamental monsoon forcing factor, and upward motion accompanied by deep cumulus convection is considered to be a direct forcing that drives vertical monsoon circulation.

It is important to remember that surface temperature warming and increase of vertical dry stability are fundamental signals obtained by the increased CO_2 event even in the vertical onedimensional radiative-convective equilibrium experiments, as well as stratospheric cooling (Manabe and Wetherald 1967).

Future changes in vertical motion are associated with future changes in upper-atmosphere circulation and winds, including the Asian monsoon circulation. As with present-day processes, some future upward velocity changes are accompanied by future precipitation changes, which are forced by a relatively warm SST (Xie et al. 2010), enhanced land–sea contrast (He et al. 2019), and changed adiabatic circulations in the mid-latitudes (e.g., Horinouchi et al. 2019). However, the future precipitation changes do not necessarily accompany the future vertical circulation changes. A unique forcing for vertical motion under a future global warming scenario is the vertically stabilized atmosphere in the sense of dry static energy, which leads to suppressed vertical motion and circulation (Vecchi and Soden 2007). He et al. (2017) suggested that the projected changes in the subtropical anticyclones are well understood by considering the combined effects of increased tropospheric static stability and changes in diabatic heating.

Near-surface atmospheric circulations can be changed directly by surface pressure distributions caused by regional surface warming. Endo et al. (2021) conducted detailed experiments to examine future changes in the seasonal progress of the East Asian monsoon circulation using the MRI-AGCM60 model. They showed that northern SST warming following northern continental summer warming is important, especially for projecting late summer climate, in addition to tropical SST pattern and globally uniform SST warming.

In this study, we used almost the same methods as those used in the previous CMIP5 study (Ose et al. 2020) by applying EOF analysis to the CMIP6 (Eyring 2016) multi-model future projections for sea-level pressure over summertime East Asia. We reconsidered the physical meaning of the CMIP6 EOF modes based on their common features and differences with respect to the CMIP5 analysis. In this paper, all results regarding the CMIP5 EOF analysis for comparison with the CMIP6 analysis come from Ose et al. (2020), unless specified otherwise.

The data used in our analysis are introduced in Section 2 and our results are described in Section 3. After discussion of the comparison with the AGCM results and possible atmospheric mechanisms in Section 4, a summary is given in Section 5.

2. Method and data used for the analysis of future projections

We analyzed the 38 models used for the CMIP6 ensemble of historical and global warming experiments under the ssp585 scenario (Table 1). We defined the difference between two sets of 20-year simulations for the present day (1980–1999) and future (2076–2095) periods as “future changes.” In this paper, we use the term “future anomaly” to indicate future changes in the individual models relative to the CMIP6 38-model ensemble mean future change. Our analytical methods followed Ose et al. (2020), and the future changes for each model were adjusted to the value at an annual mean global warming of 4 K, using the future projection of the 20-year annual global mean surface air temperature. All data used in this study were re-gridded to a resolution of 2.5° × 2.5° in longitude and latitude.

The CMIP6 results in this study are compared with those from the CMIP5 study (Ose et al. 2020), in which the 38 CMIP5 ensemble models of historical and global warming experiments under RCP 8.5 were analyzed. The CMIP6 ssp585 scenario is only one CMIP6 ssp scenario experiment with the same climate forcing as the CMIP5 RCP8.5 scenario. The periods to define the future change are different between this CMIP6 study and the previous CMIP5 one. In the latter, two sets of 25-year simulations for the present-day period from 1980 to 2004 and the future period from 2075 to 2099 are used for the future change. This difference in the analytical periods may not be crucial after the future changes in the global mean surface temperature are adjusted to 4K. Considering the same model numbers (38) of the used CMIP6 and CMIP5 projections, a two-tailed statistical test is applied in the same way: the correlation coefficients of 0.42, 0.38, 0.32 and 0.30 roughly correspond to the critical values for more than 99 %, 98 %, 95 % and 90 % significance, respectively.

The EOF analysis was applied to the East Asian EOF domain (10°–50°N, 110°–160°E) following Ose et al. (2020), which is the region used for the definition of the southerly wind index for East Asia in fig. 14.5 of IPCC (2013).

See the details of the analytical method in the Appendix.

3. Results

3.1. Sea-level pressure pattern

Future changes in the CMIP6 ensemble mean sea-level pressure (dslpMEAN) and the present-day climatology of mean sea-level pressure (slpMEAN) are shown in Fig. 1a. The dslpMEAN and slpMEAN from CMIP5 are also shown in Fig. 1b for comparison. The dslpMEAN and slpMEAN from CMIP6 are fairly similar to those from CMIP5 (hereafter referred to as dslpMEAN_CMIP5 and slpMEAN_CMIP5) over Asia and the Indo-Pacific region, including East Asia. In both CMIP6 and CMIP5, dslpMEAN is characterized by lower pressure over northern Asia and higher pressure over the tropical ocean than the present day.

The first EOF mode (dslpEOF1) explains 65.6% of the total multi-model variance of the future sea-level pressure anomalies (dslp) over the East Asian EOF domain (Fig. 2a). The inter-model correlation between dslp and dslpEOF1 resolution coefficients (dslpCOR1:see the Appendix) represents the strengthened Pacific high-pressure system expanding over the subtropical Pacific and along the continental coast from South Asia to East Asia. The dslpEOF2 (Fig. 2b) mode represents 12.7% of the total variance. The spatial pattern of dslpCOR2 shows a low-pressure anomaly over northern East Asia and a high-pressure anomaly over the tropical oceans. The dslpEOF3 (Fig. 2c) pattern is roughly reverse to the summertime climatological distribution of sea-level pressure over East Asia, indicating weakening of the southerly East Asian monsoon wind. The dslpEOF4 to dslpEOF6 modes (Fig. 2d–f) have tripolar anomalies over East Asia that explain <5% of the total variance; they show high-pressure anomalies over northern and tropical East Asia, the Okhotsk High anomaly, and a high-pressure anomaly over Japan, respectively.

Resolution coefficients of dslpEOF1-6 by the dslpEOF1-5 from the previous CMIP5 analysis (hereafter referred to as dslpEOF1-5_CMIP5: see the Appendix) are shown in Table 2. The dslpEOF1 to dslpEOF3 modes are similar to the corresponding modes from the CMIP5 (dslpEOF1_CMIP5 to dslpEOF3_CMIP5), and share >75% of the variance each other. Each variance of the dslpEOF4 and dslpEOF6 modes is broadly divided into the dslpEOF4_CMIP5 and dslpEOF5_CMIP5 modes. Note that dslpEOF6_CMIP5 (not shown) may include some variances of dslpEOF5. The analysis below concentrates on dslpEOF1 to dslpEOF3 as the similar dslpEOF patterns with the CMIP5 ensemble projections.

Figure 3 presents the contributions (resolution coefficients) of the dslpEOF1 to dslpEOF6 to each future change (not anomaly) from the 38 CMIP6 models (white bars) and the CMIP6 ensemble mean (black bars). These are normalized by the corresponding standard deviations (SD1 to SD6) for the dslpEOF1 to dslpEOF6, respectively. Specifically, the resolution coefficients (c.m.k) are calculated from Eq. (1) for the sea-level pressure anomaly of the m-th model and the k-th dslpEOF; using the notations in the Appendix,

$$\text{c.m.k} = \text{cmean.k} + \text{ca.m.k} \quad , \quad (1)$$

or

$$\text{c.m.k} = ((\text{dslpMEAN}, \text{dslpEOFk})) / \text{SDk} + ((\text{dslpa.m}, \text{dslpEOFk})) / \text{SDk} \quad , \quad (2)$$

where the double parentheses mean a calculation of the area-weighting inner product over the East Asian EOF domain.

Figure 3b confirms that every resolution coefficient for dslpEOF2 is positive, except for one model, meaning that the positive phase of dslpEOF2 pattern is robustly included in the future changes by almost all CMIP6 models. The signal-to-noise ratio (SNR), which is defined as the ensemble mean change divided by the inter-model standard deviation, is sometimes used to measure the robustness of the changes (e.g., Long and Xie 2016; Liu et al. 2019). The SNR of the dslpEOF2 coefficients is 2.06 so that the dslpEOF2 pattern are a robust pattern in the CMIP6 future projections. The SNR of the other dslpEOFs is less than 1.0; 0.33 for dslpEOF1 and 0.46, 0.66, 0.05 and 0.56 for dslpEOF3 to dslpEOF6, respectively. The result indicates that a certain number of the CMIP6 model projections include the reverse pattern of dslpEOFs except dslpEOF2. Therefore, these dslpEOFs, except dslpEOF2, represent uncertainty (or uncertain patterns) in the CMIP6 future projections. A similar tendency is evident in the CMIP5 analysis: the SNR of the coefficients for dslpEOF2_CMIP5 is 1.05, whereas the SNR is 0.54, 0.58, 0.04 and 0.09 for the dslpEOF1_CMIP5 and dslpEOF3-5_CMIP5 (table 2 in Ose et al. 2020).

The five CMIP6 models in bold font in Table 1 were selected by Shiogama et al. (2021) to widely capture the uncertainty range of the CMIP6 models over the Japanese Archipelago. They can provide better climate scenarios for impact and adaptation studies in Japan. Specifically, the four seasonal means of the 8 climate variables for the daily mean, daily maximum and minimum surface air temperatures, precipitation, surface downward shortwave and longwave radiations, surface relative humidity and surface wind speed are used to examine the good performance of the present climate simulation and the wide range covering of the future change uncertainty.

The contributions by the dslpEOFs to the five models are shown separately on the right of Fig. 3a–f. Comparing the ensemble mean and variability of the resolution coefficients for the 1st to 3rd dslpEOFs and the 4th to 6th dslpEOFs between the selected five models and the 38 CMIP6 models, the selected five models are confirmed as an appropriate small ensemble covering wide spatial ranges of near-surface circulation changes of the 38 CMIP6 multi-model ensemble.

3.2. Surface air temperature and precipitation

Surface air temperature and precipitation changes are important climatic elements within the global warming experiments, especially considering their socio-economic importance. The ensemble mean future change in surface temperature distribution (dtasMEAN in Fig. 4a) is similar to that of the CMIP5 (dtasMEAN_CMIP5). Furthermore, in both CMIP6 and CMIP5, dslpEOF2 is highly correlated with the northern continental surface air temperature anomalies (dtasCOR2 in Fig. 4c).

Future anomalies in surface air temperature (dtasCOR1 and dtasCOR3) are shown in Fig. 4b and d, differ from the corresponding CMIP5 analysis. The future CMIP5 projections of the western North Pacific subtropical high (WNPSH), corresponding to dslpEOF1 in this study, were understood to be linked to future SST changes (e.g., He and Zhou 2015; Chen et al. 2020; Ose et al. 2020; Zhou et al.

2020). The dtasCOR1 distribution shows a negative tendency in the equatorial eastern Pacific (i.e., La-Niña-like SST anomaly), whereas the negative tendency in the northwestern Pacific of dtasCOR1_CMIP5 (i.e., El-Niño-like SST anomaly) was recognized as the cause of dslpEOF1_CMIP5 by Ose et al. (2020). A reasoned explanation of the impact of the SST difference on dslpEOF1 will be given in the next subsection.

The dtasCOR3 pattern shows some positive SST anomalies in the subtropical northwestern Pacific whereas there is a very weakly correlated anomaly south of the Japanese Archipelago for dtasCOR3_CMIP5. The dslpEOF3 structure expanding toward the subtropical Pacific is more similar to the reversed pattern of the present-day climatological high sea-level pressure than that of the dslp_EOF3_CMIP5 concentrated within the mid-latitudes. The positive SST anomaly of dtasCOR3 may be interpreted as the result of weakened surface wind and evaporation over the subtropical ocean.

Figure 5a shows the ensemble mean future precipitation change (dprMEAN), which is similar to that of dprMEAN_CMIP5 but with intensified negative future changes over the oceans in Southeast Asia and smaller changes in northern East Asia. A significantly negative dprCOR1 is clear in the subtropical northwestern Pacific and along the equatorial central Pacific, and a positive dprCOR1 is distributed along the equatorial Indian Ocean from the maritime continent as well as western Asia (Fig. 5b). A similar pattern was found in dprCOR1_CMIP5, except there was no negative anomaly over the equatorial central Pacific. Negative dprCOR1 anomalies can be found significantly over central China and weakly over the Japanese Archipelago, but there is only a very weak negative anomaly around Japan in dprCOR1_CMIP5 for the June to August (JJA) mean. The major common signals of dprCOR2 and dprCOR2_CMIP5 are positive anomalies southeast of Japan and around the equatorial Pacific dateline (Fig. 5c). The similarity between dprCOR3 and dprCOR3_CMIP5 is observed in negative anomalies over northern and southern China and northern South Asia, and positive anomalies in Southeast Asia and the North Pacific around 160°W (Fig. 5d).

The correlation between dslpEOFs and the present-day precipitation (prCORs) in Fig. 5a–d will be discussed later.

3.3. Vertical velocity at 500 hPa and zonal wind at 200 hPa

Figure 6a shows the CMIP6 ensemble mean future changes in the 500-hPa vertical pressure–velocity (negative/positive for upward/downward motion) and the present-day climatology (dw500MEAN and w500MEAN). Note the expected fact that the distributions of prMEAN and prCORs in Fig. 5 well capture the features of w500MEAN and w500CORs in Fig. 6. Major downward changes (positive dw500MEAN) are found in the wet area of present-day upward motion (negative w500MEAN) over Southeast Asia and the eastern Indian Ocean, indicating downward changes forced by the future stabilized tropical atmosphere. Major upward changes are found in the downward climatology of present-day dry regions in western and central Asia. Enhanced upward changes are detected in the equatorial central Pacific, the subtropical northwestern Pacific, continental South Asia including the high mountains (He et al. 2019), and part of the Arabian Sea, where the increase in precipitation is projected possibly by forcing factors such as future SST distribution, forced circulation changes, and increased land–sea heat contrast. The above qualitative distribution of dw500MEAN was also evident in dw500MEAN_CMIP5.

The distribution of dw500COR1 (Fig. 6b) is essentially similar to that of the dw500COR1_CMIP5; i.e., downward motion anomalies over the northwestern Pacific, and upward motion anomalies over the equatorial Indian Ocean and relatively dry land from the Middle East to northwestern South Asia. Upward anomalies along the equatorial Indian Ocean from the maritime continent overlap over some areas with the present-day downward anomalies; therefore, they can be considered forced anomalies caused by the future stabilized atmosphere. The difference from the CMIP5 analysis is observed in the equatorial Pacific: downward motion anomalies occur over the equatorial central Pacific for dw500COR1 rather than over the equatorial western Pacific in dw500COR1_CMIP5. However, this difference is consistent with the negative SST anomalies in the equatorial central Pacific for dtasCOR1 (Fig. 4b), which contrasts with the negative SST anomalies in the equatorial western Pacific for dtasCOR1_CMIP5.

The tropical distribution of dw500COR2 (Fig. 6c) shows some differences to that of dw500COR2_CMIP5, reflecting the different tropical structures between dslpEOF2 and dslpEOF2_CMIP5. Future downward motion anomalies of dw500COR2 occur in the present-day upward motion anomalies (w500COR2) over the western Pacific and the northern Indian Ocean, whereas future upward motion anomalies of dw500COR2 are located in the present-day downward motion anomalies (w500COR2) over the equatorial western Indian Ocean and around the equatorial dateline. The above relationship between dw500COR2 and w500COR2 indicates that the future anomalies of dw500COR2 are also caused by the future stabilization of the tropical atmosphere.

The similarities between dw500COR3 (Fig. 6d) and dw500COR3_CMIP5 are observed in the downward motion over the northern Indian Ocean, such as the Arabian Sea and the Bay of the Bengal, and upward motion over Southeast Asia and the central North Pacific around 160°W, 35°N. These future anomalies occur mostly over the reverse present-day anomalies of w500COR3, indicating a relationship with the vertically stabilized atmosphere in the future again. The downward motion anomalies in northern continental South Asia may be accompanied by weakened near-surface circulation anomalies over the continent indicated by dslpCOR3. Similar downward motion anomalies are observed in dw500COR3_CMIP5.

Figure 7a presents the CMIP6 ensemble mean future changes in the 200-hPa zonal wind (du200MEAN) and its present-day climatology (u200MEAN). The du200MEAN is similar to that of CMIP5, except that the future decrease in the East Asian jet stream is found in lower latitudes.

The distribution of du200COR1 (Fig. 7b) is also similar to that of the CMIP5, but its magnitude is significantly weaker, especially in East Asia. The significant tropical westerly anomalies between the equatorial Indian Ocean and the equatorial Pacific are a common feature of du200COR1 and du200COR1_CMIP5. However, its longitudinal location for du200COR1 is shifted toward the Pacific by ~20° relative to that of du200COR1_CMIP5. This is consistent with the different locations of the downward motion anomalies of dw500COR1 from those of dw500COR1_CMIP5, reflecting the different longitudes of the negative SST anomalies in the equatorial central Pacific of dtasCOR1 and the equatorial western Pacific of dtasCOR1_CMIP5.

The weakened westerly or easterly anomalies over the northern landmass of du200COR2 (Fig. 7c) are similar to those of du200COR2_CMIP5, but with relatively stronger signals. Significant zonal wind anomalies are also observed in the tropics for du200COR2, but there are no corresponding anomalies in du200COR2_CMIP5; this follows the differing distributions of dw500COR2 and dw500COR2_CMIP5.

Considering du200COR3 (Fig. 7d) as an upper atmospheric response to dw500COR3, the du200COR3 reflects a weakened Asian monsoon responding to weakened upward motion (downward anomalies) over the northern Indian Ocean, such as the Arabian Sea and the Bay of Bengal, and a weakened North Pacific high pressure responding to weakened downward motion (upward anomalies) over the North Pacific around 30°–40°N, 160°W.

4. Discussion

4.1. Comparison with AGCM experiments

The contributions of dslpEOF2 to the future changes are positive for all CMIP6 projections except one model, and their ensemble mean is around double SD2 (Fig. 3b). Therefore, we can say that dslpEOF2 represents a robust change in the sea-level pressure pattern of the future summertime

East Asia. The dslpEOF2 mode is characterized by a significant relationship with the warm northern continents, as shown in dtasCOR2, whereas the other dslpEOFs show no clear connection with the warming over the continents.

The major features of dslpEOF2 have some similarity to the AGCM60 experiment anomalies shown in fig. 11i of Endo et al. (2021), in which only the future greenhouse gas effect was applied to AGCM60, while keeping the present-day SST climatology, to clarify the effects of future warming land over East Asia. The similarity of dslpEOF2 to the AGCM60 experiment anomalies is specifically in the anomalous northern low pressure and southwesterly wind over northern East Asia. We expect the effects of the northern SST changes shown in fig. 11u of Endo et al. (2020) to also be included in dslpEOF2, considering the warming extent of dtasCOR2 over the northern oceans.

4.3. Atmospheric mechanisms

The model dependences of the dslpEOF1 and dslpEOF3 contributions to the future changes introduce some uncertainty into the future multi-model sea-level pressure pattern projections. Their model dependence originally comes from the model-dependent distribution of the suppressed vertical motion in the vertically stabilized atmosphere over the globally warming oceans. Explanation for the responses of the East Asian circulation anomalies or pressure anomalies to the suppressed vertical motions may be necessary.

A relatively lower pressure anomaly can be recognized along the equatorial Indian Ocean in dslpCOR1, compared with high pressure anomalies over the subtropical northwestern and tropical western Pacific. Xie et al. (2009) suggested an atmospheric mechanism for the Indo-western Pacific climate during the summer following El Niño events, where the high-pressure anomaly over the summertime northwestern Pacific is created by the low-pressure anomaly caused by the increased precipitation and upward motion over the warm Indian Ocean. These pressure anomaly patterns and the causal upward motion anomaly over the equatorial Indian Ocean are essentially similar to those of dslpCOR1, although the details of their locations and extents are not exactly the same besides the differences between the timescales of year-to-year variability and global warming. Therefore, the dslpEOF1 and dslpCOR1 can be explained by the atmospheric mechanism for the Indo-western Pacific climate during the summer (Xie et al. 2009). We can suppose that during the northern summer, the El Nino-like and La Nina-like SST anomalies in the Pacific are not necessarily a key probably due to the climatological seasonal shift of the major convections to the Indo-western Pacific from the equatorial Pacific.

The mechanical experiment by Ting (1994) that investigated the present-day climatological northern summer stationary waves in an AGCM may help us to explain the dslpEOF3 and dslpCOR3 patterns. The results shown in fig. 13a of Ting (1994) indicate that the diabatic heating and associated upward motion limited to South Asia forms the climatological Asian monsoon near-surface pressure pattern comprising a near-surface low-pressure system over the Eurasian Continent and a near-surface high-pressure system centered over the northwestern Pacific. The equation used was linear, so the downward motion anomaly of dw500COR3 over South Asia is expected to create a reverse pattern similar to dslpCOR3.

5. Summary

The future changes in summertime East Asian sea-level pressure were investigated by applying the inter-model EOF method to the CMIP6 multi-model future projections in the same way as in previous CMIP5 analysis (Ose et al. 2020). Sources of the inter-model EOF modes were studied by examining the relationship of the EOF modes with future changes in surface air temperature, precipitation, vertical motion, and upper zonal winds over the Asia and Pacific regions. Focusing on the features that were common or different with respect to the previous CMIP5 analysis (Ose et al. 2020), the major EOF modes can be understood using the following integrated explanation.

We consider dslpEOF2 of the inter-model EOF modes to be the robust pattern for future CMIP6 projections because the contribution of dslpEOF2 to every future change simulated by almost all the CMIP6 models is positive. The robust mode of the future sea-level pressure changes consists of low pressure over northern East Asia and high pressure over southern East Asia. The greater surface warming of the summertime northern continents and the neighboring regions is closely correlated with dslpEOF2, and this is the source of the formation of the northern low pressure in the robust dslpEOF2 mode. The suppressed upward motion over the present-day wet monsoon regions (Fig. 5c), such as the subtropical northwestern Pacific and the South China Sea, contributes to creating the high pressure over southern East Asia.

The other EOF modes, including dslpEOF1 and dslpEOF3, make model-dependent contributions to the future changes and are recognized as introducing uncertainty into the future projections. These non-robust or uncertain EOF modes are derived from seesaws of the opposite vertical motion anomalies over the Indian Ocean and the Pacific.

The dslpEOF1 mode represents the subtropical high-pressure anomalies over East Asia. This can be attributed to the Walker circulation anomalies with the opposite vertical motion anomalies over the equatorial Indian Ocean and the equatorial Pacific: the upward (downward) motion anomalies over the equatorial Indian Ocean are formed in the vertically stabilized atmosphere for the models that simulate the present-day small (large) upward motion in the relatively less (more) precipitation climatology (Fig. 5b) for the positive (negative) phase of dslpEOF1. The downward (upward) motion anomalies over the equatorial Pacific develop over the relatively cold (warm) SST anomalies (Fig. 4b). The mechanism following the inter-annual Indo-western Pacific atmospheric anomaly in the post-El Niño summer (Xie et al. 2009) is suggested as the cause for the East Asian subtropical high-pressure anomalies and associated downward motion anomalies of dslpEOF1.

The dslpEOF3 is similar to the reverse anomalies of the climatological pressure pattern in summertime East Asia. The positive (negative) phase of the mode is related to the suppressed (enhanced) upward motion anomalies in the relatively wet (dry) present-day monsoon climatology (Fig. 5d) over the northern Indian Ocean, such as the Bay of the Bengal and the Arabian Sea. Opposite processes occur in the northern Pacific; i.e., suppressed (enhanced) downward motion anomalies over the relatively dry (wet) present-day climatology (Fig. 5d). We suggest that the mechanism for dslpEOF3 is basically the same as that for the summertime stationary waves produced by the monsoon diabatic heating over South Asia only (Ting 1994).

Major differences from the CMIP5 analysis are observed in the SST anomalies related to the dslpEOFs. However, their major characteristics, including the basic structures and sources, are not affected, although the SST anomalies are related to the secondary structures of the dslpEOFs.

The results regarding the robust pattern from the land warming and the uncertain patterns from the vertical motion anomalies over the oceans are reasonable because, in general, the warming process over land is determined relatively simply by modeling of the land surface energy budget, whereas the vertical motion process over the oceans involves much more complicated modeling, such as ocean circulation, atmospheric convection, and SST in the ocean surface flux budget.

The suppressed vertical motion anomalies or changes by the vertically stabilized atmosphere under global warming are closely related to the present-day precipitation climatology in the model simulations (w500CORs in Fig. 5 and prCORs in Fig. 6). This may lead to the possibility that the uncertainty associated with the dslpEOFs could be reduced by comparing the modeled and observed precipitation climatology.

The higher modes of the dslpEOFs have fine structures, which are not necessarily the same as the higher modes from the CMIP5 analysis (Table 2), but they include the modes correlated closely with the future changes in local precipitation and temperature over East Asia. The summertime monthly relationships of some dslpEOFs with temperature and precipitation anomalies were different in the CMIP5 analysis. Studies of the higher modes and the monthly details may also lead to more useful future projections.

High-resolution models can simulate tropical cyclones in a realistic way, so the future changes in tropical cyclones may make qualitatively and/or quantitatively different contributions to the future changes in seasonal and monthly mean atmospheric circulations (Ito et al. 2020). We wish multi-model projections using high-resolution climate models in the next.

Data Availability Statement

The CMIP5/6 model data used in this study can be accessed at the ESGF portal (https://esgf-node.llnl.gov/projects/esgf-llnl/).

Acknowledgments

This work was supported by the Environment Research and Technology Development Fund (JPMEERF20192004) of the Environmental Restoration and Conservation Agency of Japan. We acknowledge the World Climate Research Program's Working Group on Coupled Modeling, which is responsible for CMIP6, and climate modeling groups worldwide for producing and making available their model output. We also acknowledge the University of Tokyo through a project “Research hub for the big data analysis of global water cycle and precipitation in changing climate” and Osamu Arakawa in JAMSTEC for the use of the model output data on 2.5x2.5 grids. We also thank the editor and two anonymous reviewers for their comments helpful in improving the manuscripts.

Appendix

The future change of sea-level pressure in the m-th CMIP6 model (dslp.m.i) and its anomaly (dslpa.m.i) from the CMIP6 ensemble mean sea-level pressure (dslpMEAN.i) at i-th grid point of the East Asian EOF domain are related as follows; using the total number of the models (M=38) and the notation of Σ.m for the summation from m=1 to m=M,

$$\mathrm{dslp.m.i} = \mathrm{dslpMEAN.i} + \mathrm{dslpa.m.i} \quad , \quad \text{(A1)}$$

$$\mathrm{dslpMEAN.i} = (\Sigma\mathrm{.m\ dslp.m.i})/\ M \quad . \quad \text{(A2)}$$

The EOF analysis is applied to the covariance matrix (A) of the future changes of the area-weighting sea-level pressure over the East Asian EOF domain;

$$\mathrm{A.i.j} = \Sigma\mathrm{.m}\ [\mathrm{dslpa.m.i} \times \cos(\mathrm{lat.i})] \times [\mathrm{dslpa.m.j} \times \cos(\mathrm{lat.j})]\ /\mathrm{M} \quad , \quad \text{(A3)}$$

where the suffix of i and j represents the i-th and j-th grids in the domain, and lat.i and lat.j represent their latitudes.

Various coefficients (Ca, Cmean, ca and cmean) are defined in the association with the k-th normalized EOF of the sea-level pressures (dslpEOF.k.i). Using the notation of Σ.k for the summation from k=1 to k=K,

$$\mathrm{dslpa.m.i} = \Sigma\mathrm{.k}\ (\mathrm{Ca.m.k} \times \mathrm{dslpEOF.k.i}) \quad , \quad \text{(A4)}$$

$$\mathrm{dslpMEAN.i} = \Sigma\mathrm{.k}\ (\mathrm{Cmean.k} \times \mathrm{dslpEOF.k.i}) \quad , \quad \text{(A5)}$$

$$\mathrm{dslp.m.i} = \Sigma\mathrm{.k}\ [\ (\mathrm{Cmean.k} + \mathrm{Ca.m.k}) \times \mathrm{dslpEOF.k.i}\ ] \quad , \quad \text{(A6)}$$

$$(\mathrm{SD.k})^2 = \Sigma\mathrm{.m}\ (\mathrm{Ca.m.k})^2\ /\ \mathrm{M} \quad , \quad \text{(A7)}$$

$$\mathrm{dslp.m.i} = \Sigma\mathrm{.k}\ [\ \mathrm{SD.k} \times (\mathrm{cmean.k} + \mathrm{ca.m.k}) \times \mathrm{dslpEOF.k.i}\ ] \quad . \quad \text{(A8)}$$

Likewise, for any fields (f.i) over the globe, including sea-level pressure, the future change in the m-th CMIP6 model projection (df.m.i) and its anomaly (dfa.m.i) from the CMIP6 ensemble mean field (dfMEAN.i), and its anomaly correlation with dslpEOF.k.i (dfCOR.k.i) are defined.

$$\mathrm{df.m.i} = \mathrm{dfMEAN.i} + \mathrm{dfa.m.i} \quad , \quad \text{(A9)}$$

$$\mathrm{dfMEAN.i} = (\Sigma\mathrm{.m\ df.m.i})\ /\ \mathrm{M} \quad , \quad \text{(A10)}$$

$$dfCOR.k.i = \Sigma.m\ (Ca.m.k \times dfa.m.i) / (SD.k) / (Sdfa.i) / M \quad , \qquad (A11)$$

or

$$dfCOR.k.i = \Sigma.m\ (ca.m.k \times dfa.m.i) / (Sdfa.i) / M \quad , \qquad (A12)$$

where

$$(Sdfa.i)^2 = \Sigma.m\ (dfa.m.i)^2 / M \quad . \qquad (A13)$$

In the text, the notations with the suffix of i, k and m may be omitted or generalized. For examples in the case of k=3 and f=tas, the notations such as “dslpEOF3”, “dtasMEAN”, “dtasCOR3” and “SD3” are used instead of “dslpEOF.3.i“, “dtasMEAN.i”, “dtasCOR.3.i” and “SD.3”. The same statistical variables but from the CMIP5 case are denoted such as “dslpEOF3_CMIP5”, “dtasMEAN_CMIP5”, “dtasCOR3_CMIP5” and “SD3_CMIP5”.

References

Chen, X., T. Zhou, P. Wu, Z. Guo, and M. Wang, 2020: Emergent constraints on future projections of the western North Pacific Subtropical High. *Nat. Commun.*, doi:10.1038/s41467-020-16631-9.

Endo, H., A. Kitoh, R. Mizuta, and T. Ose, 2021: Different future changes between early and late summer monsoon precipitation in East Asia. *J. Meteor. Soc. Japan*, 96, 1501-1524, doi:10.2151/jmsj.2021-073.

Endo, H., A. Kitoh, and H. Ueda, 2018: A unique feature of the Asian summer monsoon response to global warming: the role of different land-sea thermal contrast change between the lower and upper troposphere. *SOLA*, 14, 57-63, doi:10.2151/sola.2018-010.

Eyring, V., S. Bony, G. A. Meehl, C. A. Senior, B. Stevens, R. J. Stouffer, and K. E. Taylor, 2016: Overview of the coupled model inter comparison project phase 6 (CMIP6) experimental design and organization. *Geosci. Model Dev.*, 9, 1937–1958, doi:10.5194/gmd-9-1937-2016.

He C, Zhou W., 2020: Different enhancement of the East Asian summer monsoon under global warming and Interglacial Epochs simulated by CMIP6 models: role of the subtropical high. *J. Climate* **33**, 9721-9733. doi:10.1175/jcli-d-20-0304.1.

He, C., Z. Wang, T. Zhou, and T. Li, 2019: Enhanced latent heating over the Tibetan Plateau as a key to the enhanced East Asian summer monsoon circulation under a warming climate. *J. Climate*, **32**, 3373–3388.

He, C., B. Wu, L. Zou, and T. Zhou, 2017: Responses of the summertime subtropical anticyclones to global warming. *J. Climate*, **30**, 6465–6479.

He, C. and T. Zhou, 2015: Responses of the western North Pacific subtropical High to global warming under RCP4.5 and RCP8.5 scenarios projected by 33 CMIP5 models: the dominance of tropical Indian Ocean-tropical western Pacific SST gradient. *J. Climate*, 28, 365-380, doi: 10.1175/JCLI-D-13-00494.1.

Held, I. M., and B. J. Soden, 2006: Robust responses of the hydrological cycle to global warming. *J. Climate*, **19**, 5686–5699.

Horinouchi, T., S. Matsumura, T. Ose, and Y. N. Takayabu, 2019: Jet-precipitation relation and future change of the Mei-Yu-Baiu rainband and subtropical jet in CMIP5 coupled GCM simulations. *J. Climate*, **32**, 2247–2259.

IPCC, 2013: Climate Change 2013: the physical science basis. Contribution of working group I to the fifth assessment report of the intergovermental panel on climate change. Stocker T. F., Qin D., Plattner G. K., Tignor M., Allen S. K., Boschung J., Nauels A., Xia Y., Bex V., Midgley P. M. (eds.) Cambridge University Press, Cambridge, pp.1535.

Ito, R., T. Ose, H. Endo, R. Mizuta, K. Yoshida, A. Kitoh, T. Nakaegawa, 2020: Seasonal characteristics of future climate change over Japan and the associated atmospheric circulation anomalies in global model experiments. *Hydro. Res. Lett.*, **14**, 130-135, doi:10.3178/hrl.14.130.

Kamae Y, Watanabe M, Kimoto M, Shiogama H, 2014: Summertime land–sea thermal contrast and atmospheric circulation over East Asia in a warming climate—Part II: Importance of CO2-induced continental warming. *Climate Dyn*., 43, 2569-2583, doi:10.1007/s00382-014-2146-0.

Kitoh, A., S. Yukimoto, A. Noda, and T. Motoi, 1997: Simulated changes in the Asian summer monsoon at times of increased atmospheric CO2. *J. Meteor. Soc. Japan*, **75**, 1019-1031.

Kimoto, M., 2005: Simulated change of the east Asian circulation under global warming scenario. *Geophys. Res. Lett.*, 32, L16701, doi:10.1029/2005GL023383.

Liu, Y, Y. Li and Ding, Y., 2020: East Asian summer rainfall projection and uncertainty under a global warming scenario. *Int. J. Climatol.*, **40**, 4828–4842, doi:10.1002/joc.6491.

Long, S.-M., S.-P. Xie and W. Liu, 2016: Uncertainty in tropical rainfall projections: atmospheric circulation effect and the ocean coupling. *J. Climate*, **29**, 2671–2687.

Manabe S. and R. T. Weatherald, 1967: Thermal equilibrium of the atmosphere with a given distribution of relative humidity. *J. Atmos. Sci.*, **24**, 241-259.

Mizuta, R., H. Yoshimura, H. Murakami, M. Matsueda, H.Endo, T. Ose, K. Kamiguchi, M. Hosaka, M. Sugi, S.Yukimoto, S. Kusunoki, and A. Kitoh, 2012: Climate simulations using MRI-AGCM3.2 with 20-km grid. *J. Meteor. Soc. Japan*, **90A**, 233–258.

Ose, T., Y. Takaya, S. Maeda, and T. Nakaegawa, 2020: Resolution of summertime East Asian pressure pattern and southerly monsoon wind in CMIP5 multi-model future projections. *J. Meteor. Soc. Japan*, **98**, 927-944, doi:10.2151/jmsj.2020-047.

Ose, T., 2017: Future precipitation changes during summer in East Asia and model dependence in high-resolution MRI-AGCM experiments. *Hydro. Res. Lett.*, **11**, 168-174, doi:10.3178/hrl.11.168.

Shepherd T.G., 2019: Storyline approach to the construction of regional climate change 303 information. *Proc. Roy. Soc. A*, **475**, 20190013.

Shiogama, H., N. N. Ishizaki, N. Hanasaki, K. Takahashi, S. Emori, R. Ito, T. Nakaegawa, I. Takayabu, Y. Hijioka, Y. N. Takayabu, R. Shibuya, 2021: Selecting CMIP6-Based Future Climate Scenarios for Impact and Adaptation Studies. *SOLA*, 17, 57-62, doi:10.2151/sola.2021-009.

Taylor, K.E., R.J. Stouffer, G.A. Meehl, 2012: An Overview of CMIP5 and the experiment design. *Bull. Amer. Meteor. Soc.*, **93**, 485-498.

Ting, M., 1994: Maintenance of northern summer stationary waves. *J. Atmos. Sci.*, **51**, 3286-3308.

Ueda, H., A. Iwai, K. Kuwano, and M. E. Hori, 2006: Impact of anthropogenic forcing on the Asian summer monsoon as simulated by eight GCMs. *Geophys. Res. Lett.*, **33**, L06703, doi:10.1029/2005GL025336.

Vecchi, G. A., and B. J. Soden, 2007: Global warming and the weakening of the tropical circulation. *J. Climate*, **20**, 4316–4340.

Xie, S.-P., C. Deser, G. A. Vecchi, J. Ma, H. Teng, and A. T. Wittenberg, 2010: Global warming pattern formation: sea surface temperature and rainfall. *J. Climate*, **23**, 966-986.

Xie, S.-P., K. Hu, J. Hafner, H. Tokinaga, Y. Du, G. Huang, and T. Sampe, 2009: Indian Ocean capacitor effect on Indo–western Pacific climate during the summer following El Niño. *J. Climate*, **22**, 730-747.

Zhou, S., G. Huang, and P. Huang, 2020: Inter-model spread of the changes in the East Asian summer monsoon system in CMIP5/6 models. *J. Geophys. Res.: Atmos.*, **125**, doi:10.1029/2020JD033016.

Zhou, S., G. Huang, and P. Huang, 2017: Changes in the East Asian summer monsoon rainfall under global warming: moisture budget decomposition and the sources of uncertainty. *Climate Dyn.*, doi: 10.1007/s00382-017-3959-4.

Figure legends

Fig. 1. (a) Future change in CMIP6 ensemble mean sea-level pressure (colors: hPa) and the present-day mean sea-level pressure relative to 1000 hPa (contours every 4 hPa) for JJA. (b) As (a), but for the CMIP5 ensemble mean.

Fig. 2. (a) Inter-model correlations of future sea-level pressure anomalies with the coefficients of dslpEOF1 (colors). Contours within the East Asian EOF region (110°–160°E and 10°–50°N) represent dslpEOF1 multiplied by its standard deviation for every 0.2 hPa. The percentage in the top-right corner represents the ratio of the variance explained by dslpEOF1. (b)–(f) As (a), but for dslpEOF2–dslpEOF6, respectively.

Fig. 3. (a) Resolution coefficients of future changes in the East Asian sea-level pressure into dslpEOF1 on the vertical axis using units normalized by the standard derivation of the dslpEOF1 variance (hPa). Figures from 1 to 38 for empty bars in the horizontal axis represent the model numbers of the 38 CMIP6 models in Table 1. Black bars are the 38-model CMIP6 ensemble mean of the coefficient. Figures from 40 to 44 and the five red bars are the five selected CMIP6 models (Table 1), and figure 45 and the green bar are their ensemble mean. (b)–(f) As (a), but for dslpEOF2–dslpEOF6, respectively.

Fig. 4. (a) Future changes in CMIP6 ensemble mean surface air temperature (colors: °C) and its present-day climatology (contours every 10°C) for JJA. (b) Inter-model correlations of the future surface air temperature anomalies with the coefficient of dslpEOF1 (colors) and the CMIP6 ensemble mean of the surface air temperature changes (contours every 1°C). (c) and (d) As (b), but for the dslpEOF2 and dslpEOF3, respectively.

Fig. 5. (a) Future changes in CMIP6 ensemble mean precipitation (colors: mm day^{-1}) and its present-day climatology (contours of 1, 2, 4, 8, 12, 16, 20, and 24 mm day^{-1}) for JJA. (b) Inter-model correlations of the future precipitation anomalies (colors) and the present-day precipitation anomalies (contours for 0.3 and -0.3 and every 0.2 but for 0.0) with the coefficient of dslpEOF1. (c) and (d) As (a), but for dslpEOF2 and dslpEOF3, respectively.

Fig. 6. (a) Future changes in CMIP6 ensemble mean 500-hPa pressure-velocity (colors: hPa hour^{-1}) and its present-day climatology (contours every 0.8 hPa hour^{-1}) for JJA. Positive/negative pressure–velocity indicates downward/upward motion. (b) Inter-model correlations of the 500-hPa pressure–velocity anomalies in the future (colors) and present-day climatology (contours for 0.3 and -0.3 and every 0.2 but for 0.0) with the coefficient of dslpEOF1. (c) and (d) As (b), but for dslpEOF2 and dslpEOF3, respectively.

Fig. 7. (a) Future changes in CMIP6 ensemble mean 200-hPa zonal wind (colors: m s^{-1}) and its present-day climatology (contours every 10 m s^{-1}) for JJA. (b) Inter-model correlations of the future 200-hPa zonal wind anomalies with the coefficient of dslpEOF1 (colors) and future changes in the CMIP6 ensemble mean (contours every 1.0 m s^{-1}). (c) and (d) As (b), but for dslpEOF2 and dslpEOF3, respectively.

Table legends

Table 1: The 38 CMIP6 models used. Names in bold in the "Model" column are the five CMIP6 models selected by Shiogama et al. (2021). The format in the "Member" column indicates the model-dependent identifier of realization or ensemble member (r), initialization method (i), physics (p) and forcing (f), which is used to distinguish the member of each model experiments (see https://es-doc.org/cmip6/).

Table 2: Resolution coefficients of the normalized dslpEOF1 to dslpEOF6 from CMIP6 into the normalized dslpEOF1 to dslpEOF5 from CMIP5. Figures in bold indicate more than 0.5 or less than –0.5.

Table 1: The 38 CMIP6 models used. Names in bold in the "Model" column are the five CMIP6 models selected by Shiogama et al. (2021). The format in the "Member" column indicates the model-dependent identifier of realization or ensemble member (r), initialization method (i), physics (p) and forcing (f), which is used to distinguish the member of each model experiments (see https://es-doc.org/cmip6/).

No	Model	Member	Institution
1	**ACCESS-CM2**	r1i1p1f1	CSIRO-ARCCSS (CSIRO and Australian Research Council Centre of Excellence for Climate System Science), Australia
2	ACCESS-ESM1-5	r1i1p1f1	CSIRO (Commonwealth Scientific and Industrial Research Organisation,), Australia
3	AWI-CM-1-1-MR	r1i1p1f1	AWI (Alfred Wegener Institute), Germany
4	BCC-CSM2-MR	r1i1p1f1	BCC (Beijing Climate Center), China
5	CAMS-CSM1-0	r1i1p1f1	CAMS (Chinese Academy of Meteorological Sciences), China
6	CanESM5	r1i1p1f1	CCCMa (Canadian Centre for Climate Modelling and Analysis), Canada
7	CESM2	r1i1p1f1	National Center for Atmospheric Research, USA
8	CESM2-WACCM	r1i1p1f1	National Center for Atmospheric Research, USA
9	CMCC-CM2-SR5	r1i1p1f1	CMCC (Centro Euro-Mediterraneo sui Cambiamenti Climatici), Italy
10	CNRM-CM6-1-HR	r1i1p1f2	CNRM (Centre National de Recherches Meteorologiques) and CERFACS (Centre Europeen de Recherche et Formation Avancees en Calcul Scientifique), France
11	CNRM-CM6-1	r1i1p1f2	CNRM and CERFACS, France
12	CNRM-ESM2-1	r1i1p1f2	CNRM and CERFACS, France
13	EC-Earth3	r1i1p1f1	EC-Earth consortium, Europe
14	EC-Earth3-Veg	r1i1p1f1	EC-Earth consortium, Europe
15	FGOALS-f3-L	r1i1p1f1	CAS (Institute of Atmospheric Physics, Chinese Academy of Sciences), China
16	FGOALS-g3	r1i1p1f1	CAS, China
17	FIO-ESM-2-0	r1i1p1f1	FIO-QNLM (First Institute of Oceanography, and Pilot National Laboratory for Marine Science and Technology, Qingdao) China
18	GFDL-CM	r1i1p1f1	NOAA-GFDL (National Oceanic and Atmospheric Administration, Geophysical Fluid Dynamics Laboratory), USA
19	GFDL-ESM4	r1i1p1f1	NOAA-GFDL, USA
20	GISS-E2-1-G	r1i1p1f2	NASA-GISS (Goddard Institute for Space Studies), USA
21	HadGEM3-GC31-LL	r1i1p1f3	MOHC (Met Office Hadley Centre), UK
22	HadGEM3-GC31-MM	r1i1p1f3	MOHC

23	IITM-ESM	r1i1p1f1	CCCR-IITM (Centre for Climate Change Research, Indian Institute of Tropical Meteorology), India
24	INM-CM4-8	r1i1p1f1	INM (Institute for Numerical Mathematics), Russia
25	INM-CM5-0	r1i1p1f1	INM, Russia
26	**IPSL-CM6A-LR**	r1i1p1f1	IPSL（Institut Pierre-Simon Laplace）, France
27	KACE-1-0-G	r1i1p1f1	NIMS-KMA (National Institute of Meteorological Sciences, Korea Meteorological Administration), Korea
28	MCM-UA-1-0	r1i1p1f2	University of Arizona, USA
29	**MIROC6**	r1i1p1f1	MIROC (Model for Interdisciplinary Research on Climate) consortium (JAMSTEC; Japan Agency for Marine-Earth Science and Technology, AORI; Atmosphere and Ocean Research Institute; NIES, National Institute for Environmental Studies; RCCS, RIKEN Center for Computational Science), Japan
30	MIROC-ES2L	r1i1p1f2	MIROC consortium, Japan
31	**MPI-ESM1-2-HR**	r1i1p1f1	MPI-M (Max Planck Institute for Meteorology), Germany
32	MPI-ESM1-2-LR	r1i1p1f1	MPI-M, Germany
33	**MRI-ESM2-0**	r1i1p1f1	MRI (Meteorological Research Institute), Japan
34	NESM3	r1i1p1f1	NUIST (Nanjing University of Information Science and Technology), China
35	NorESM2-LM	r1i1p1f1	NCC (NorESM Climate Modeling Consortium), Norway
36	NorESM2-MM	r1i1p1f1	NCC, Norway
37	TaiESM1	r1i1p1f1	AS-RCEC (Research Center for Environmental Changes, Academia Sinica), Taiwan
38	UK-ESM1-0-LL	r1i1p1f2	MOHC

The data for 500-hPa vertical velocity of MCM-UA-1-0 was unavailable on our hands in this study.

Table 2: Resolution coefficients of the normalized dslpEOF1 to dslpEOF6 from CMIP6 into the normalized dslpEOF1 to dslpEOF5 from CMIP5. Figures in bold indicate more than 0.5 or less than –0.5.

	dslpEOF1 _CMIP5	dslpEOF2 _CMIP5	dslpEOF3 _CMIP5	dslpEOF4 _CMIP5	dslpEOF5 _CMIP5
dslpEOF1	**0.926**	-0.334	0.086	0.045	0.066
dslpEOF2	0.351	**0.873**	0.036	0.113	-0.168
dslpEOF3	-0.086	0.102	**0.906**	0.111	-0.227
dslpEOF4	0.040	0.148	0.238	**-0.751**	**0.548**
dslpEOF5	0.009	0.172	-0.063	-0310.	-0.275
dslpEOF6	0.057	-0.170	-0.114	-0.412	**-0.514**

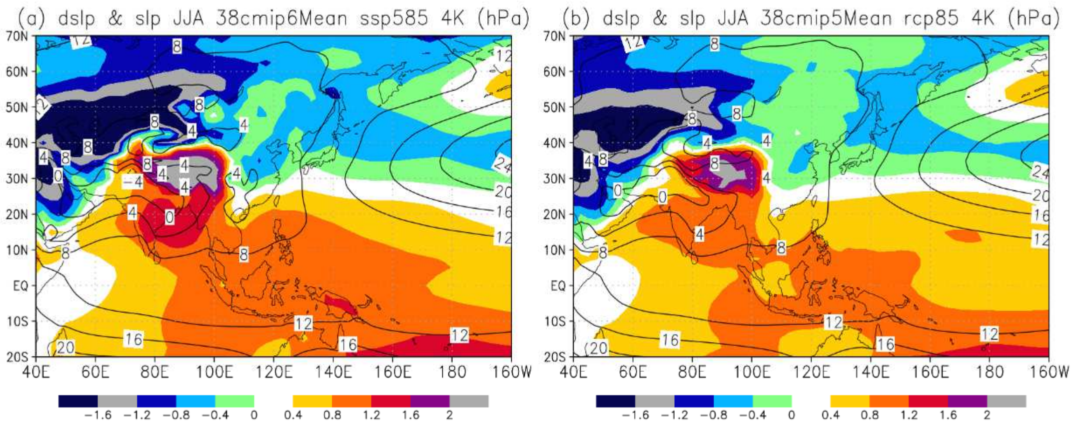

Fig. 1. (a) Future change in CMIP6 ensemble mean sea-level pressure (colors: hPa) and the present-day mean sea-level pressure relative to 1000 hPa (contours every 4 hPa) for JJA. (b) As (a), but for the CMIP5 ensemble mean.

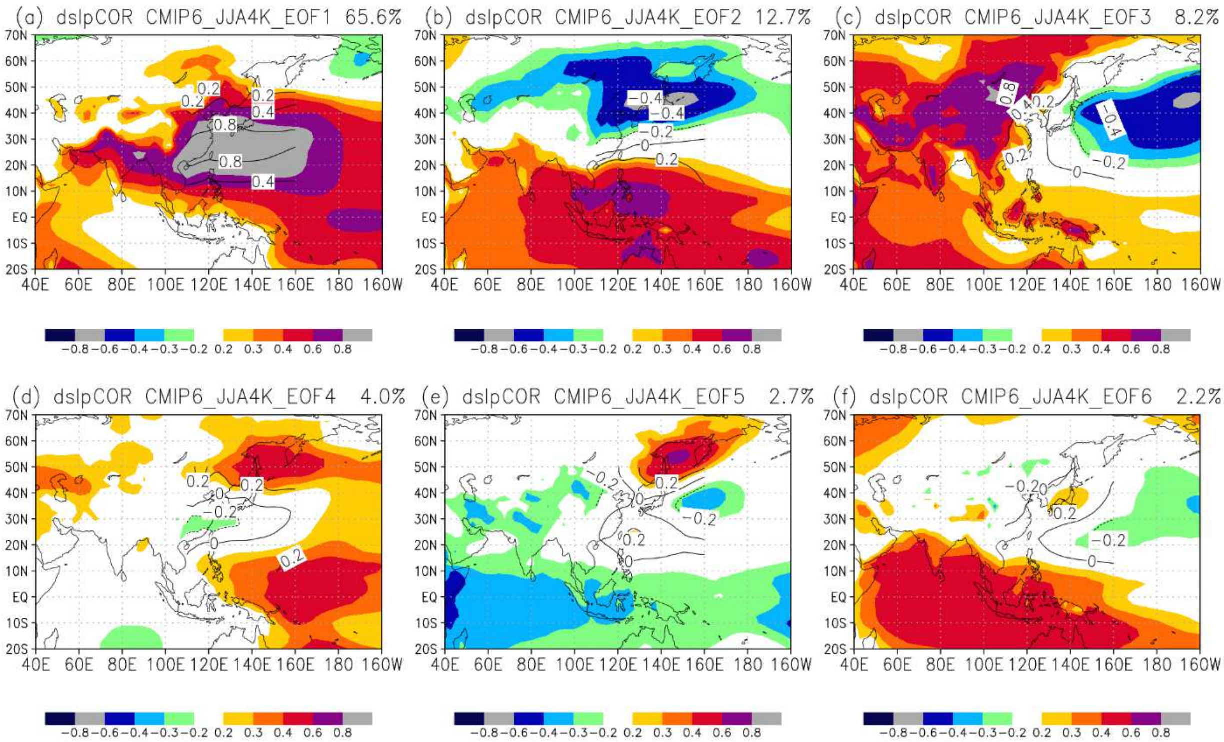

Fig. 2. (a) Inter-model correlations of future sea-level pressure anomalies with the coefficients of dslpEOF1 (colors). Contours within the East Asian EOF region (110°–160°E and 10°–50°N) represent dslpEOF1 multiplied by its standard deviation for every 0.2 hPa. The percentage in the top-right corner represents the ratio of the variance explained by dslpEOF1. (b)–(f) As (a), but for dslpEOF2–dslpEOF6, respectively.

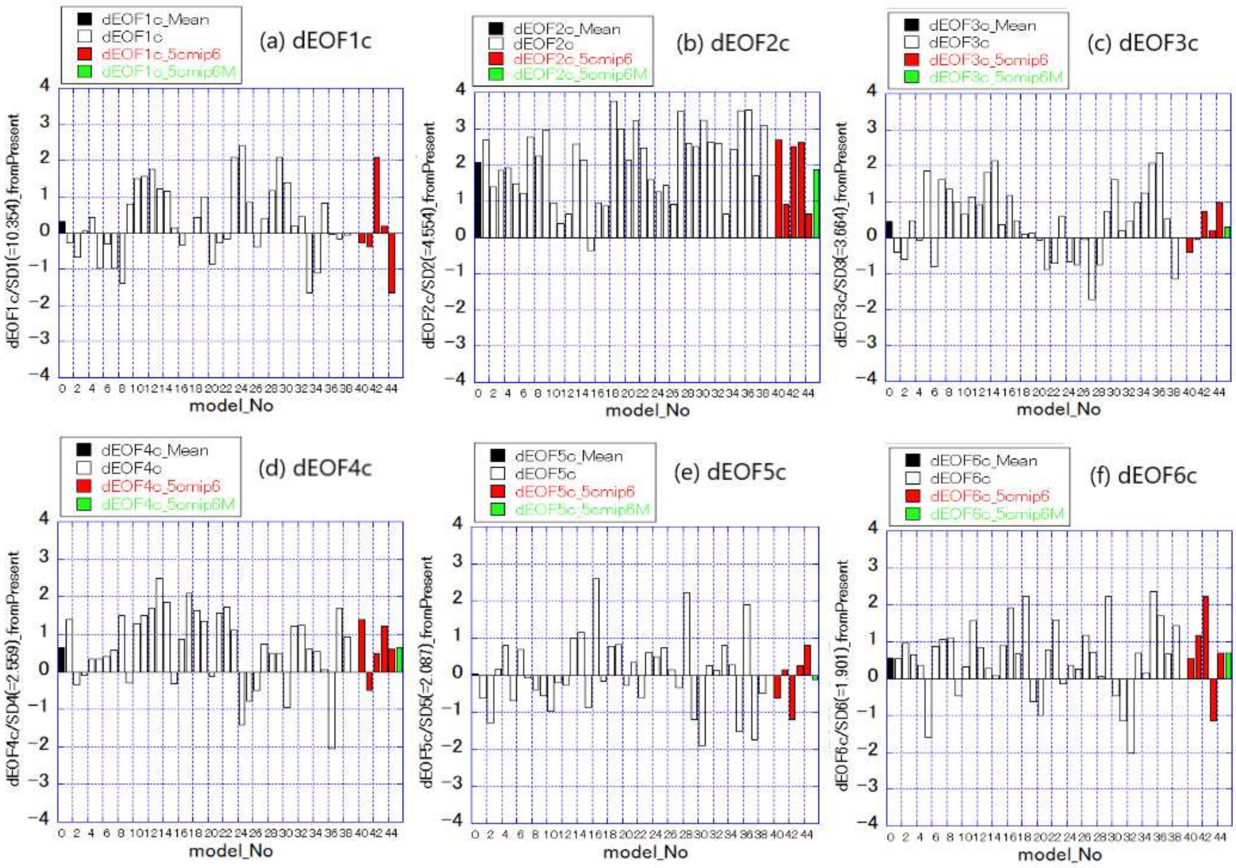

Fig. 3. (a) Resolution coefficients of future changes in the East Asian sea-level pressure into dslpEOF1 on the vertical axis using units normalized by the standard derivation of the dslpEOF1 variance (hPa). Figures from 1 to 38 for empty bars in the horizontal axis represent the model numbers of the 38 CMIP6 models in Table 1. Black bars are the 38-model CMIP6 ensemble mean of the coefficient. Figures from 40 to 44 and the five red bars are the five selected CMIP6 models (Table 1), and figure 45 and the green bar are their ensemble mean. (b)–(f) As (a), but for dslpEOF2–dslpEOF6, respectively.

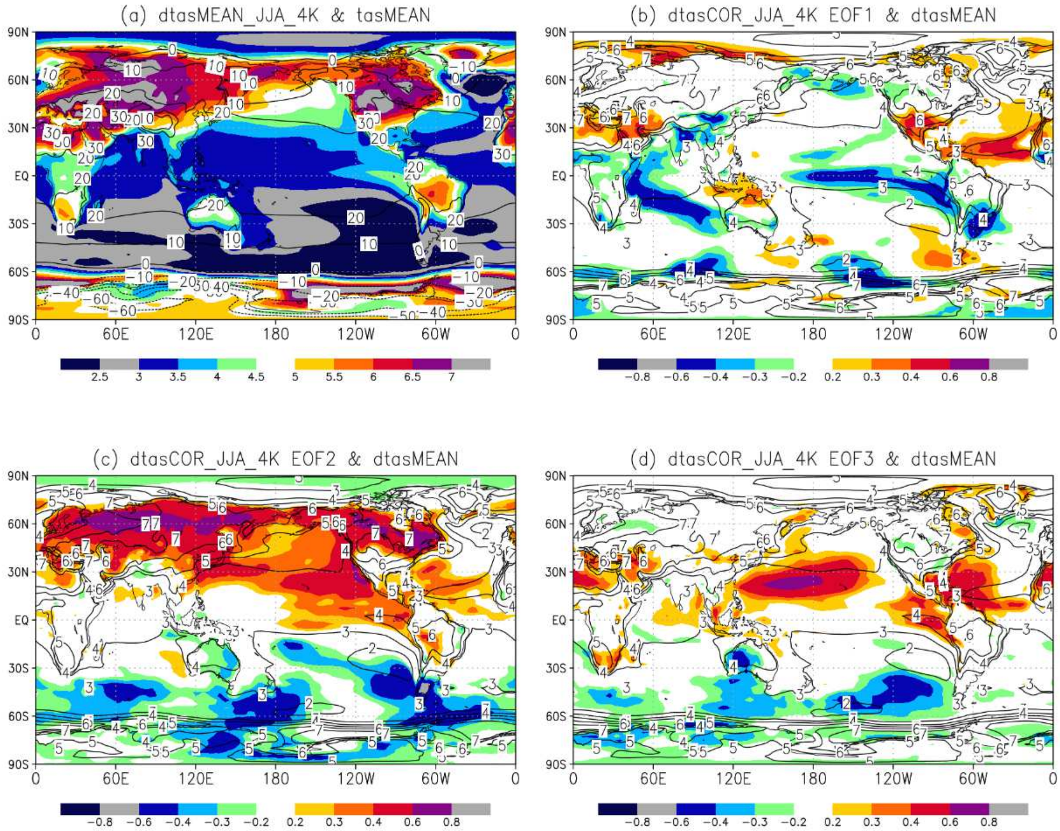

Fig. 4. (a) Future changes in CMIP6 ensemble mean surface air temperature (colors: °C) and its present-day climatology (contours every 10°C) for JJA. (b) Inter-model correlations of the future surface air temperature anomalies with the coefficient of dslpEOF1 (colors) and the CMIP6 ensemble mean of the surface air temperature changes (contours every 1°C). (c) and (d) As (b), but for the dslpEOF2 and dslpEOF3, respectively.

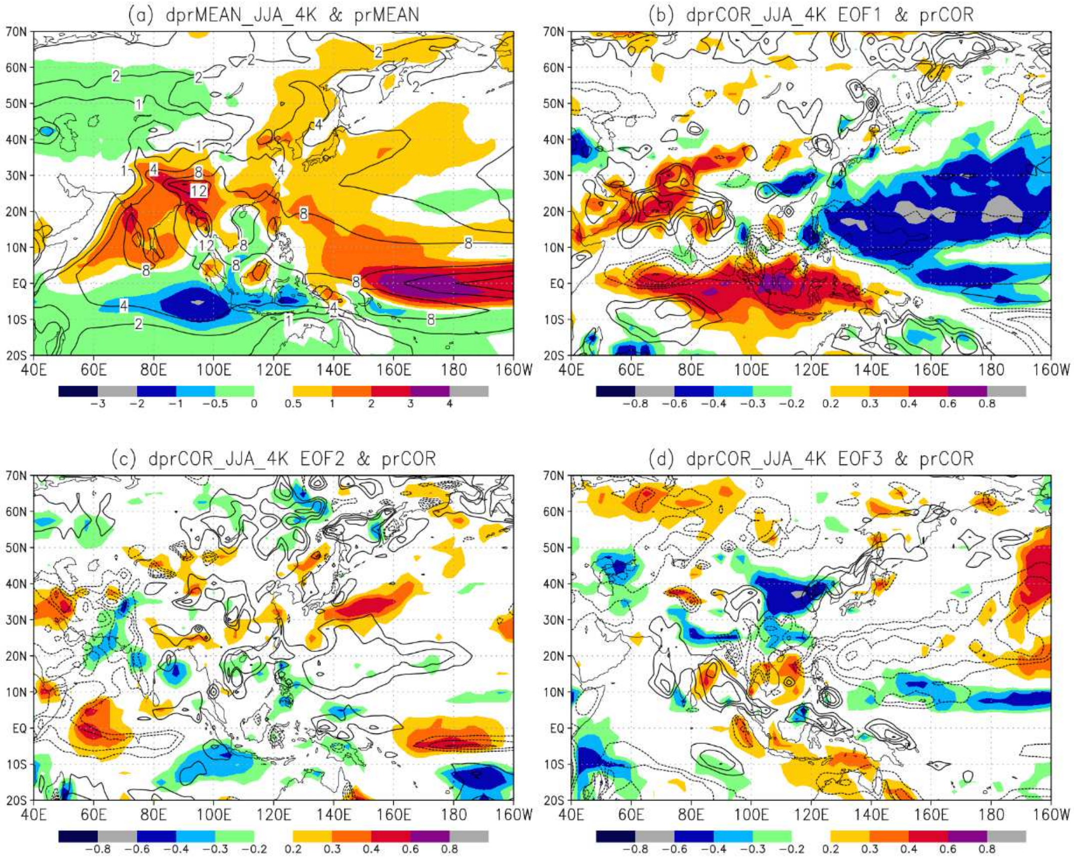

Fig. 5. (a) Future changes in CMIP6 ensemble mean precipitation (colors: mm day^{-1}) and its present-day climatology (contours of 1, 2, 4, 8, 12, 16, 20, and 24 mm day^{-1}) for JJA. (b) Inter-model correlations of the future precipitation anomalies (colors) and the present-day precipitation anomalies (contours for 0.3 and -0.3 and every 0.2 but for 0.0) with the coefficient of dslpEOF1. (c) and (d) As (a), but for dslpEOF2 and dslpEOF3, respectively.

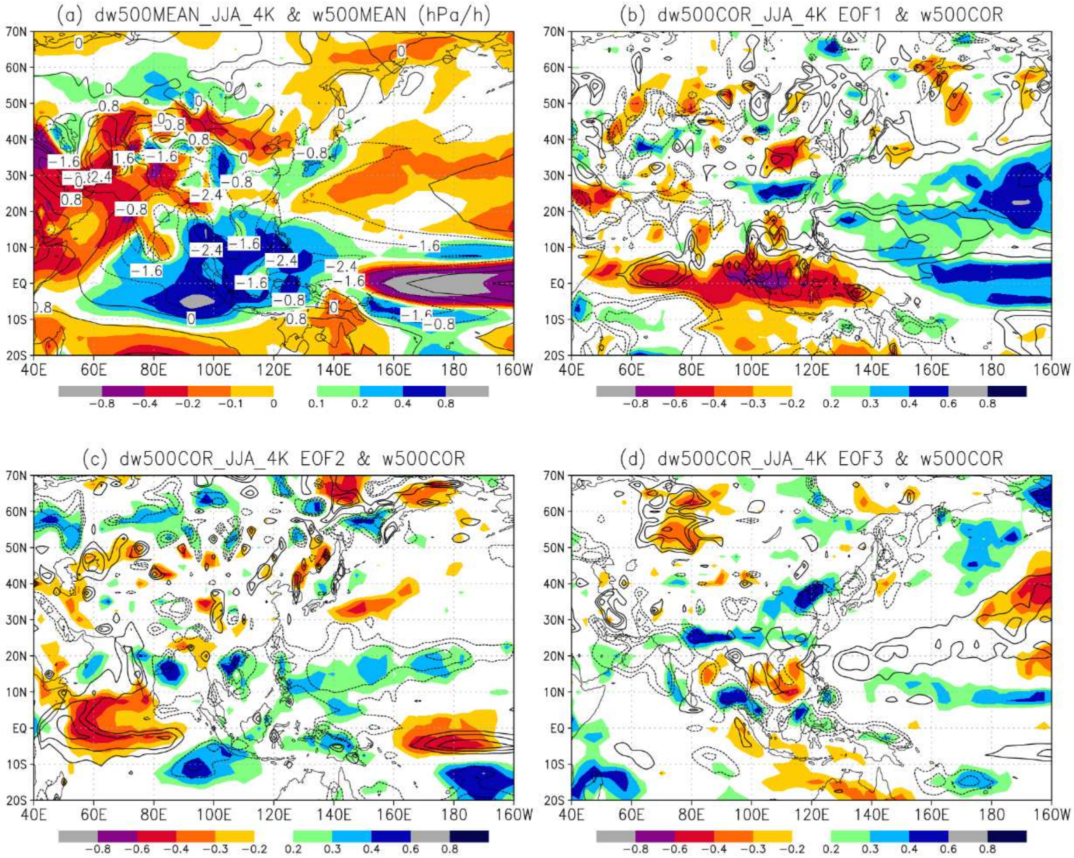

Fig. 6. (a) Future changes in CMIP6 ensemble mean 500-hPa pressure-velocity (colors: hPa hour^{-1}) and its present-day climatology (contours every 0.8 hPa hour^{-1}) for JJA. Positive/negative pressure–velocity indicates downward/upward motion. (b) Inter-model correlations of the 500-hPa pressure–velocity anomalies in the future (colors) and present-day climatology (contours for 0.3 and -0.3 and every 0.2 but for 0.0) with the coefficient of dslpEOF1. (c) and (d) As (b), but for dslpEOF2 and dslpEOF3, respectively.

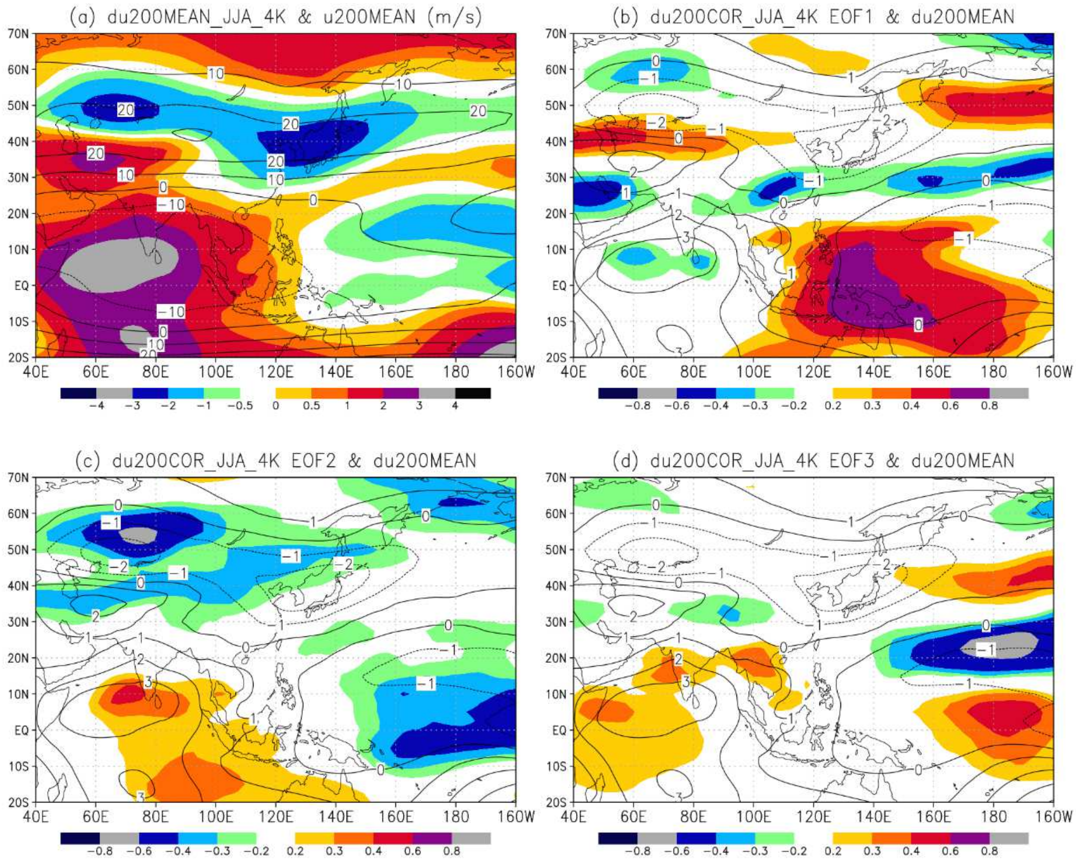

Fig. 7. (a) Future changes in CMIP6 ensemble mean 200-hPa zonal wind (colors: m s^{-1}) and its present-day climatology (contours every 10 m s^{-1}) for JJA. (b) Inter-model correlations of the future 200-hPa zonal wind anomalies with the coefficient of dslpEOF1 (colors) and future changes in the CMIP6 ensemble mean (contours every 1.0 m s^{-1}). (c) and (d) As (b), but for dslpEOF2 and dslpEOF3, respectively.